



Measurement of the branching fraction, polarization, and CP asymmetry in $B^0 \rightarrow \rho^+ \rho^-$ decays

K. Abe,⁹ K. Abe,⁴⁷ I. Adachi,⁹ H. Aihara,⁴⁹ K. Aoki,²³ K. Arinstein,² Y. Asano,⁵⁴
T. Aso,⁵³ V. Aulchenko,² T. Aushev,¹³ T. Aziz,⁴⁵ S. Bahinipati,⁵ A. M. Bakich,⁴⁴
V. Balagura,¹³ Y. Ban,³⁶ S. Banerjee,⁴⁵ E. Barberio,²² M. Barbero,⁸ A. Bay,¹⁹ I. Bedny,²
U. Bitenc,¹⁴ I. Bizjak,¹⁴ S. Blyth,²⁵ A. Bondar,² A. Bozek,²⁹ M. Bračko,^{9, 21, 14}
J. Brodzicka,²⁹ T. E. Browder,⁸ M.-C. Chang,⁴⁸ P. Chang,²⁸ Y. Chao,²⁸ A. Chen,²⁵
K.-F. Chen,²⁸ W. T. Chen,²⁵ B. G. Cheon,⁴ C.-C. Chiang,²⁸ R. Chistov,¹³ S.-K. Choi,⁷
Y. Choi,⁴³ Y. K. Choi,⁴³ A. Chuvikov,³⁷ S. Cole,⁴⁴ J. Dalseno,²² M. Danilov,¹³ M. Dash,⁵⁶
L. Y. Dong,¹¹ R. Dowd,²² J. Dragic,⁹ A. Drutskoy,⁵ S. Eidelman,² Y. Enari,²³ D. Epifanov,²
F. Fang,⁸ S. Fratina,¹⁴ H. Fujii,⁹ N. Gabyshev,² A. Garmash,³⁷ T. Gershon,⁹ A. Go,²⁵
G. Gokhroo,⁴⁵ P. Goldenzweig,⁵ B. Golob,^{20, 14} A. Gorišek,¹⁴ M. Grosse Perdekamp,³⁸
H. Guler,⁸ R. Guo,²⁶ J. Haba,⁹ K. Hara,⁹ T. Hara,³⁴ Y. Hasegawa,⁴² N. C. Hastings,⁴⁹
K. Hasuko,³⁸ K. Hayasaka,²³ H. Hayashii,²⁴ M. Hazumi,⁹ T. Higuchi,⁹ L. Hinz,¹⁹ T. Hojo,³⁴
T. Hokuue,²³ Y. Hoshi,⁴⁷ K. Hoshina,⁵² S. Hou,²⁵ W.-S. Hou,²⁸ Y. B. Hsiung,²⁸
Y. Igarashi,⁹ T. Iijima,²³ K. Ikado,²³ A. Imoto,²⁴ K. Inami,²³ A. Ishikawa,⁹ H. Ishino,⁵⁰
K. Itoh,⁴⁹ R. Itoh,⁹ M. Iwasaki,⁴⁹ Y. Iwasaki,⁹ C. Jacoby,¹⁹ C.-M. Jen,²⁸ R. Kagan,¹³
H. Kakuno,⁴⁹ J. H. Kang,⁵⁷ J. S. Kang,¹⁶ P. Kapusta,²⁹ S. U. Kataoka,²⁴ N. Katayama,⁹
H. Kawai,³ N. Kawamura,¹ T. Kawasaki,³¹ S. Kazi,⁵ N. Kent,⁸ H. R. Khan,⁵⁰
A. Kibayashi,⁵⁰ H. Kichimi,⁹ H. J. Kim,¹⁸ H. O. Kim,⁴³ J. H. Kim,⁴³ S. K. Kim,⁴¹
S. M. Kim,⁴³ T. H. Kim,⁵⁷ K. Kinoshita,⁵ N. Kishimoto,²³ S. Korpar,^{21, 14} Y. Kozakai,²³
P. Krizán,^{20, 14} P. Krokovny,⁹ T. Kubota,²³ R. Kulasiri,⁵ C. C. Kuo,²⁵ H. Kurashiro,⁵⁰
E. Kurihara,³ A. Kusaka,⁴⁹ A. Kuzmin,² Y.-J. Kwon,⁵⁷ J. S. Lange,⁶ G. Leder,¹²
S. E. Lee,⁴¹ Y.-J. Lee,²⁸ T. Lesiak,²⁹ J. Li,⁴⁰ A. Limosani,⁹ S.-W. Lin,²⁸ D. Liventsev,¹³
J. MacNaughton,¹² G. Majumder,⁴⁵ F. Mandl,¹² D. Marlow,³⁷ H. Matsumoto,³¹
T. Matsumoto,⁵¹ A. Matyja,²⁹ Y. Mikami,⁴⁸ W. Mitaroff,¹² K. Miyabayashi,²⁴ H. Miyake,³⁴
H. Miyata,³¹ Y. Miyazaki,²³ R. Mizuk,¹³ D. Mohapatra,⁵⁶ G. R. Moloney,²² T. Mori,⁵⁰
A. Murakami,³⁹ T. Nagamine,⁴⁸ Y. Nagasaka,¹⁰ T. Nakagawa,⁵¹ I. Nakamura,⁹
E. Nakano,³³ M. Nakao,⁹ H. Nakazawa,⁹ Z. Natkaniec,²⁹ K. Neichi,⁴⁷ S. Nishida,⁹
O. Nitoh,⁵² S. Noguchi,²⁴ T. Nozaki,⁹ A. Ogawa,³⁸ S. Ogawa,⁴⁶ T. Ohshima,²³ T. Okabe,²³
S. Okuno,¹⁵ S. L. Olsen,⁸ Y. Onuki,³¹ W. Ostrowicz,²⁹ H. Ozaki,⁹ P. Pakhlov,¹³ H. Palka,²⁹
C. W. Park,⁴³ H. Park,¹⁸ K. S. Park,⁴³ N. Parslow,⁴⁴ L. S. Peak,⁴⁴ M. Pernicka,¹²
R. Pestotnik,¹⁴ M. Peters,⁸ L. E. Piilonen,⁵⁶ A. Poluektov,² F. J. Ronga,⁹ N. Root,²
M. Rozanska,²⁹ H. Sahoo,⁸ M. Saigo,⁴⁸ S. Saitoh,⁹ Y. Sakai,⁹ H. Sakamoto,¹⁷
H. Sakaue,³³ T. R. Sarangi,⁹ M. Satapathy,⁵⁵ N. Sato,²³ N. Satoyama,⁴² T. Schietinger,¹⁹
O. Schneider,¹⁹ P. Schönmeier,⁴⁸ J. Schümann,²⁸ C. Schwanda,¹² A. J. Schwartz,⁵
T. Seki,⁵¹ K. Senyo,²³ R. Seuster,⁸ M. E. Sevier,²² T. Shibata,³¹ H. Shibuya,⁴⁶

J.-G. Shiu,²⁸ B. Shwartz,² V. Sidorov,² J. B. Singh,³⁵ A. Somov,⁵ N. Soni,³⁵ R. Stamen,⁹
 S. Stanič,³² M. Starič,¹⁴ A. Sugiyama,³⁹ K. Sumisawa,⁹ T. Sumiyoshi,⁵¹ S. Suzuki,³⁹
 S. Y. Suzuki,⁹ O. Tajima,⁹ N. Takada,⁴² F. Takasaki,⁹ K. Tamai,⁹ N. Tamura,³¹
 K. Tanabe,⁴⁹ M. Tanaka,⁹ G. N. Taylor,²² Y. Teramoto,³³ X. C. Tian,³⁶ K. Trabelsi,⁸
 Y. F. Tse,²² T. Tsuboyama,⁹ T. Tsukamoto,⁹ K. Uchida,⁸ Y. Uchida,⁹ S. Uehara,⁹
 T. Uglov,¹³ K. Ueno,²⁸ Y. Unno,⁹ S. Uno,⁹ P. Urquijo,²² Y. Ushiroda,⁹ G. Varner,⁸
 K. E. Varvell,⁴⁴ S. Villa,¹⁹ C. C. Wang,²⁸ C. H. Wang,²⁷ M.-Z. Wang,²⁸ M. Watanabe,³¹
 Y. Watanabe,⁵⁰ L. Widhalm,¹² C.-H. Wu,²⁸ Q. L. Xie,¹¹ B. D. Yabsley,⁵⁶ A. Yamaguchi,⁴⁸
 H. Yamamoto,⁴⁸ S. Yamamoto,⁵¹ Y. Yamashita,³⁰ M. Yamauchi,⁹ Heyoung Yang,⁴¹
 J. Ying,³⁶ S. Yoshino,²³ Y. Yuan,¹¹ Y. Yusa,⁴⁸ H. Yuta,¹ S. L. Zang,¹¹ C. C. Zhang,¹¹
 J. Zhang,⁹ L. M. Zhang,⁴⁰ Z. P. Zhang,⁴⁰ V. Zhilich,² T. Ziegler,³⁷ and D. Zürcher¹⁹

(The Belle Collaboration)

¹*Aomori University, Aomori*

²*Budker Institute of Nuclear Physics, Novosibirsk*

³*Chiba University, Chiba*

⁴*Chonnam National University, Kwangju*

⁵*University of Cincinnati, Cincinnati, Ohio 45221*

⁶*University of Frankfurt, Frankfurt*

⁷*Gyeongsang National University, Chinju*

⁸*University of Hawaii, Honolulu, Hawaii 96822*

⁹*High Energy Accelerator Research Organization (KEK), Tsukuba*

¹⁰*Hiroshima Institute of Technology, Hiroshima*

¹¹*Institute of High Energy Physics,*

Chinese Academy of Sciences, Beijing

¹²*Institute of High Energy Physics, Vienna*

¹³*Institute for Theoretical and Experimental Physics, Moscow*

¹⁴*J. Stefan Institute, Ljubljana*

¹⁵*Kanagawa University, Yokohama*

¹⁶*Korea University, Seoul*

¹⁷*Kyoto University, Kyoto*

¹⁸*Kyungpook National University, Taegu*

¹⁹*Swiss Federal Institute of Technology of Lausanne, EPFL, Lausanne*

²⁰*University of Ljubljana, Ljubljana*

²¹*University of Maribor, Maribor*

²²*University of Melbourne, Victoria*

²³*Nagoya University, Nagoya*

²⁴*Nara Women's University, Nara*

²⁵*National Central University, Chung-li*

²⁶*National Kaohsiung Normal University, Kaohsiung*

²⁷*National United University, Miao Li*

²⁸*Department of Physics, National Taiwan University, Taipei*

²⁹*H. Niewodniczanski Institute of Nuclear Physics, Krakow*

³⁰*Nippon Dental University, Niigata*

³¹*Niigata University, Niigata*

³²*Nova Gorica Polytechnic, Nova Gorica*

- ³³*Osaka City University, Osaka*
³⁴*Osaka University, Osaka*
³⁵*Panjab University, Chandigarh*
³⁶*Peking University, Beijing*
³⁷*Princeton University, Princeton, New Jersey 08544*
³⁸*RIKEN BNL Research Center, Upton, New York 11973*
³⁹*Saga University, Saga*
⁴⁰*University of Science and Technology of China, Hefei*
⁴¹*Seoul National University, Seoul*
⁴²*Shinshu University, Nagano*
⁴³*Sungkyunkwan University, Suwon*
⁴⁴*University of Sydney, Sydney NSW*
⁴⁵*Tata Institute of Fundamental Research, Bombay*
⁴⁶*Toho University, Funabashi*
⁴⁷*Tohoku Gakuin University, Tagajo*
⁴⁸*Tohoku University, Sendai*
⁴⁹*Department of Physics, University of Tokyo, Tokyo*
⁵⁰*Tokyo Institute of Technology, Tokyo*
⁵¹*Tokyo Metropolitan University, Tokyo*
⁵²*Tokyo University of Agriculture and Technology, Tokyo*
⁵³*Toyama National College of Maritime Technology, Toyama*
⁵⁴*University of Tsukuba, Tsukuba*
⁵⁵*Utkal University, Bhubaneswer*
⁵⁶*Virginia Polytechnic Institute and State University, Blacksburg, Virginia 24061*
⁵⁷*Yonsei University, Seoul*

Abstract

We have measured the branching fraction, longitudinal polarization fraction f_L , and the CP asymmetry coefficients \mathcal{A} and \mathcal{S} in $B^0 \rightarrow \rho^+\rho^-$ decays. These results are obtained from a 253fb^{-1} data sample containing 275 million $B\bar{B}$ pairs collected by the Belle detector running at the KEKB e^+e^- collider. We obtain $B = \left[24.4 \pm 2.2(\text{stat})_{-4.1}^{+3.8}(\text{syst})\right] \times 10^{-6}$, $f_L = 0.951_{-0.039}^{+0.033}(\text{stat})_{-0.031}^{+0.029}(\text{syst})$, $\mathcal{A} = 0.00 \pm 0.30(\text{stat})_{-0.09}^{+0.10}(\text{syst})$, and $\mathcal{S} = 0.09 \pm 0.42(\text{stat}) \pm 0.08(\text{syst})$. These values are used to determine the CKM phase angle ϕ_2 via an isospin analysis; the central value and 1σ error are $(87 \pm 17)^\circ$, and $59^\circ < \phi_2 < 115^\circ$ at 90% CL.

PACS numbers: 13.25.Hw, 11.30.Er, 12.15.Hh

The decay $B^0 \rightarrow \rho^+ \rho^-$ has received much attention in the literature because it allows one to determine the CKM phase angle ϕ_2 [1] with relatively little theoretical uncertainty. This is because the penguin contribution to $B^0 \rightarrow \rho^+ \rho^-$ is small, as indicated by the small branching fraction for $B^0 \rightarrow \rho^0 \rho^0$ [2]. The angle ϕ_2 is determined by measuring the decay time (Δt) distribution of B^0 and \bar{B}^0 decays; the difference between the distributions is fit to the function $\mathcal{A} \cos(\Delta m \Delta t) + \mathcal{S} \sin(\Delta m \Delta t)$, where Δm is the mass difference between the two B^0 - \bar{B}^0 mass eigenstates, and the CP asymmetry coefficients \mathcal{A} and \mathcal{S} depend on ϕ_2 . To determine ϕ_2 requires knowledge of the polarization of the ρ mesons, as different polarization amplitudes can give different values of \mathcal{A} and \mathcal{S} for the same ϕ_2 . For a negligible penguin contribution, the sign of \mathcal{S} for the CP -odd transversity amplitude A_\perp will be opposite to that for the CP -even amplitudes A_0 and A_\parallel . In this paper we present a measurement of the branching fraction, longitudinal polarization fraction (f_L), and coefficients \mathcal{A} and \mathcal{S} for $B^0 \rightarrow \rho^+ \rho^-$ decays.

The data sample consists of 253 fb⁻¹ recorded by the Belle experiment running at the KEKB energy-asymmetric e^+e^- collider [3]. The Belle detector [4] consists of a silicon vertex detector (SVD), a 50-layer central drift chamber (CDC), an array of aerogel threshold Cherenkov counters (ACC), time-of-flight scintillation counters (TOF), and an electromagnetic calorimeter comprised of CsI(Tl) crystals. These detectors are located within a superconducting solenoid coil providing a 1.5 T magnetic field. An iron flux-return located outside the coil is instrumented to identify muons and detect K_L^0 mesons. Two inner detector configurations were used: a 2.0 cm beampipe and a 3-layer silicon vertex detector were used for the first sample of 152 million $B\bar{B}$ pairs, and a 1.5 cm beampipe, a 4-layer silicon detector, and a small-cell inner drift chamber were used for the remaining 123 million $B\bar{B}$ pairs [5].

Candidate $B^0 \rightarrow \rho^+ \rho^-$, $\rho^\pm \rightarrow \pi^\pm \pi^0$ decays are selected by requiring two oppositely-charged tracks satisfying $p_T > 0.10$ GeV/ c , $dr < 2.0$ mm, and $|dz| < 4.0$ cm, where p_T is the momentum transverse to the beam axis, and dr and dz are the radial and longitudinal distances, respectively, between the track and the beam crossing point. The tracks are fit to a common vertex, and the resulting χ^2 is required to be satisfactory. We require that the tracks be identified as pions based on information from the TOF and ACC systems, and from dE/dx measurement in the CDC. This information is combined into a likelihood for a track to be a pion (L_π) or a kaon (L_K). To identify pions, we require that the ratio $L_K/(L_K + L_\pi)$ be less than 0.40. The efficiency of this requirement is approximately 89%, and the kaon misidentification rate is about 10%. Tracks are rejected if they satisfy an electron identification criterion based on information from the ECL system.

The π^\pm candidates are subsequently combined with π^0 candidates. The latter are reconstructed from pairs of photons having an invariant mass in the range 0.1178–0.1502 GeV, which corresponds to $\pm 3\sigma$ in π^0 mass resolution. The energy of each photon in the laboratory frame must be > 50 (90) MeV in the ECL barrel (endcap) region, which subtends the angular range with respect to the beamline of 32°–129° (17°–32° and 129°–150°). In order to reduce combinatorial background, π^0 candidates are required to have $p > 0.35$ GeV/ c in the e^+e^- center-of-mass (CM) frame. To identify $\rho^\pm \rightarrow \pi^\pm \pi^0$ decays, we require that $m_{\pi^\pm \pi^0}$ be in the range 0.62–0.92 GeV/ c^2 ; this window corresponds to $\pm 2\sigma$ in the $\pi^\pm \pi^0$ mass distribution. To further reduce combinatorial background, we require that each ρ candidate satisfy $-0.80 < \cos \theta < 0.98$, where θ is the angle between the direction of the π^0 and the negative of the B^0 momentum in the ρ^\pm rest frame.

To select $B^0 \rightarrow \rho^+ \rho^-$ decays, we calculate the quantities $M_{bc} \equiv \sqrt{E_{\text{beam}}^2 - p_B^2}$ and

$\Delta E \equiv E_B - E_{\text{beam}}$, where E_B and p_B are the reconstructed energy and momentum of the B candidate, and E_{beam} is the beam energy, all evaluated in the CM frame. The ΔE distribution has a long tail on the lower side due to incomplete containment of the electromagnetic shower in the ECL. We define a signal region $5.27 \text{ GeV}/c^2 < M_{\text{bc}} < 5.29 \text{ GeV}/c^2$ and $-0.12 \text{ GeV} < \Delta E < 0.08 \text{ GeV}$. The fraction of events having multiple candidates in this region is 9.5%. Many of these arise from fake π^0 's combining with good tracks, and thus we choose the best candidate based on the mass difference $|m_{\gamma\gamma} - m_{\pi^0}|$. From MC simulation we find that this criterion correctly identifies the $B^0 \rightarrow \rho^+\rho^-$ decay 87% (95%) of the time for longitudinal (transverse) polarization. Signal decays that have one or more daughters incorrectly identified but nonetheless pass all selection requirements are referred to as ‘‘self-cross-feed’’ (SCF) background. Most such decays have the π^0 daughter swapped with a π^0 originating from the rest of the event; this preserves the vertex position and thus the Δt value.

We identify whether a B^0 or \bar{B}^0 evolved and decayed to $\rho^+\rho^-$ by tagging the b flavor of the non-signal (opposite-side) B decay in the event. This is done using a tagging algorithm [6] that categorizes charged leptons, kaons, and Λ 's found in the event. The algorithm returns two parameters: q , which equals +1 (−1) when the opposite-side B is likely to be a B^0 (\bar{B}^0); and r , which represents the quality of the tag as determined from MC simulation and varies from $r=0$ for no flavor discrimination to $r=1$ for unambiguous flavor assignment.

The dominant background is $e^+e^- \rightarrow q\bar{q}$ ($q = u, d, s, c$) continuum production. We discriminate against this using event topology: $e^+e^- \rightarrow q\bar{q}$ processes in the CM frame tend to be jet-like, while $e^+e^- \rightarrow B\bar{B}$ events tend to be spherical. To quantify this sphericity, we calculate a set of 16 modified Fox-Wolfram moments and combine them into a Fisher discriminant [7]. We calculate a probability density function (PDF) based on this discriminant and multiply it by a PDF for $\cos\theta_B$, where θ_B is the polar angle in the CM frame between the B direction and the positron beam direction. $B\bar{B}$ events are produced with a $1 - \cos^2\theta_B$ distribution while continuum events are produced uniformly in $\cos\theta_B$. The PDFs for signal and continuum background are obtained using MC simulation and the data sideband $5.21 \text{ GeV}/c^2 < M_{\text{bc}} < 5.26 \text{ GeV}/c^2$, respectively. We use the products of the PDFs to calculate a signal likelihood \mathcal{L}_s and continuum likelihood $\mathcal{L}_{q\bar{q}}$ and require that $\mathcal{R} = \mathcal{L}_s/(\mathcal{L}_s + \mathcal{L}_{q\bar{q}})$ be above a threshold. This threshold is determined by optimizing a figure-of-merit $N_S/\sqrt{N_S + N_B}$, where N_S (N_B) is the number of signal (background) events estimated to be in the signal region from MC simulation (extrapolating from an M_{bc} sideband). For this calculation we assume a $B^0 \rightarrow \rho^+\rho^-$ branching fraction of 25×10^{-6} . As the tagging parameter r also discriminates against $q\bar{q}$ background, we divide the data into six r intervals (denoted by $\ell = 1-6$) and determine the \mathcal{R} threshold separately for each. The \mathcal{R} requirement removes about 97% of continuum events while retaining about 62% of $B^0 \rightarrow \rho^+\rho^-$ signal. The efficiency of all selection criteria as determined from MC simulation is $(2.19 \pm 0.02)\%$. This value corresponds to $f_L = 1$; the efficiency for our measured value of f_L (which is slightly less than one – see below) is about 4% higher, and we include this difference as an additional systematic error in the branching fraction.

We determine the signal yield in two steps: we first fit the $M_{\text{bc}}-\Delta E$ distribution to obtain the fraction of $B^0 \rightarrow \rho^+\rho^- + B^0 \rightarrow \rho^\pm\pi^\mp\pi^0$ non-resonant decays (as this fit cannot distinguish between the two modes); we then fit the $m_{\pi^\pm\pi^0}$ distribution to determine the non-resonant fraction and hence the $\rho^+\rho^-$ signal yield.

The first fit is an unbinned maximum likelihood (ML) fit to the two-dimensional $M_{\text{bc}}-\Delta E$ distribution in the wide range $5.21 \text{ GeV}/c^2 < M_{\text{bc}} < 5.29 \text{ GeV}/c^2$ and $-0.20 \text{ GeV} < \Delta E <$

0.30 GeV. The fit includes components for the signal and several backgrounds: continuum events, $b \rightarrow c$ decays, and $b \rightarrow u$ decays. The PDFs for signal and $b \rightarrow u$ background are modeled by smoothed two-dimensional histograms obtained from large MC samples. The PDF for $b \rightarrow c$ background is the product of a threshold (“ARGUS” [8]) function for M_{bc} and a quadratic polynomial for ΔE , also obtained from MC simulation. The PDF for continuum background is taken to be an ARGUS function for M_{bc} and a linear function for ΔE ; the slope of the linear function depends on the tag quality (r) bin ℓ , and all seven shape parameters are floated in the fit. The signal PDF is adjusted to account for small differences observed between data and MC for a high-statistics sample of $B^+ \rightarrow \overline{D}^0 \rho^+$, $\overline{D}^0 \rightarrow K^+ \pi^- \pi^0$ decays, which, like the signal mode, contain two neutral pions.

The $b \rightarrow u$ background is dominated by $B^{(0,+)} \rightarrow \rho \pi$, $B \rightarrow a_1 \pi$, and $B \rightarrow a_1 \rho$ decays. As their contributions are small, their normalization is fixed to the yield obtained from MC simulation. For $B^+ \rightarrow a_1^+ \pi^0$ and $B \rightarrow a_1 \rho$, the branching fractions are unknown; we therefore estimate them to be 3×10^{-6} and 2×10^{-6} , respectively, and vary these values by 50% and 100%, respectively, to obtain the systematic error due to these estimates. There are thus nine free parameters in the fit, and the resulting fraction of $B^0 \rightarrow \rho^+ \rho^- + \text{non-resonant decays}$ in the signal region is $(3.0 \pm 0.4)\%$. Figure 1 shows the final event sample and projections of the fit result. The χ^2 of the projections divided by the number of bins is 0.97 for M_{bc} and 1.02 for ΔE .

To distinguish $B^0 \rightarrow \rho^+ \rho^-$ decays from non-resonant $B^0 \rightarrow \rho^\pm \pi^\mp \pi^0$ and $B^0 \rightarrow \pi^+ \pi^0 \pi^- \pi^0$ decays, we do an unbinned ML fit to the $\pi^\pm \pi^0$ mass distribution. For this fit we require $5.27 \text{ GeV}/c^2 < M_{bc} < 5.29 \text{ GeV}/c^2$ and $-0.12 \text{ GeV} < \Delta E < 0.08 \text{ GeV}$ and fit the $m_{\pi^\pm \pi^0}$ distribution in the range 0.30–1.80 GeV/c^2 . Only one ρ candidate is required to satisfy $0.62 \text{ GeV}/c^2 < m_{\pi^\pm \pi^0} < 0.92 \text{ GeV}/c^2$; the mass of the other ρ candidate is then fit. We include additional PDFs for non-resonant $B \rightarrow \rho \pi \pi$ and $B \rightarrow \pi \pi \pi \pi$ components; however, the fit result for the latter is negligibly small ($\ll 1\%$) and consistent with zero, and thus we set this fraction to zero. The PDFs for continuum and $b \rightarrow c$ backgrounds are grouped together and taken from the data sideband $5.22 \text{ GeV}/c^2 < M_{bc} < 5.26 \text{ GeV}/c^2$; we use MC simulation to check that the shapes of these backgrounds and their ratio in the sideband region are very close to those in the signal region. We impose the constraint that the fraction of signal + non-resonant events in the $m_{\pi^\pm \pi^0}$ range 0.62–0.92 GeV/c^2 equals that which we obtained from the M_{bc} - ΔE fit; there is then only one free parameter in the fit ($f_{\rho\pi\pi}$). The result of the fit is $f_{\rho\pi\pi} = (8.9 \pm 6.2)\%$, and thus $N_{\rho\rho} = 142 \pm 13$ events. Figure 2 shows the data (two entries per event) and the projection of the fit result. The χ^2 of the projection divided by the number of bins is 1.35.

The branching fraction is evaluated as

$$B(B^0 \rightarrow \rho^+ \rho^-) = \frac{N_{\rho\rho}}{\varepsilon \cdot \varepsilon_{\text{PID}} \cdot N_{B\overline{B}}}, \quad (1)$$

where $N_{\rho\rho}$ is the number of $B^0 \rightarrow \rho^+ \rho^-$ candidates (142 ± 13), $N_{B\overline{B}}$ is the number of $B\overline{B}$ pairs produced $[(274.8 \pm 2.3) \times 10^6]$, ε is the geometric acceptance and efficiency of selection criteria obtained from MC simulation $[(2.19 \pm 0.02)\%]$, and ε_{PID} is a correction factor for the pion identification requirement to account for small differences between data and MC (0.969 ± 0.012). Inserting these values into Eq. (1) gives a branching fraction of $(24.4 \pm 2.2) \times 10^{-6}$, where the error given is statistical.

There are several sources of systematic uncertainty; their effect is evaluated by varying the relevant parameter(s) by $\pm 1\sigma$ and noting the resulting change in the branching fraction.

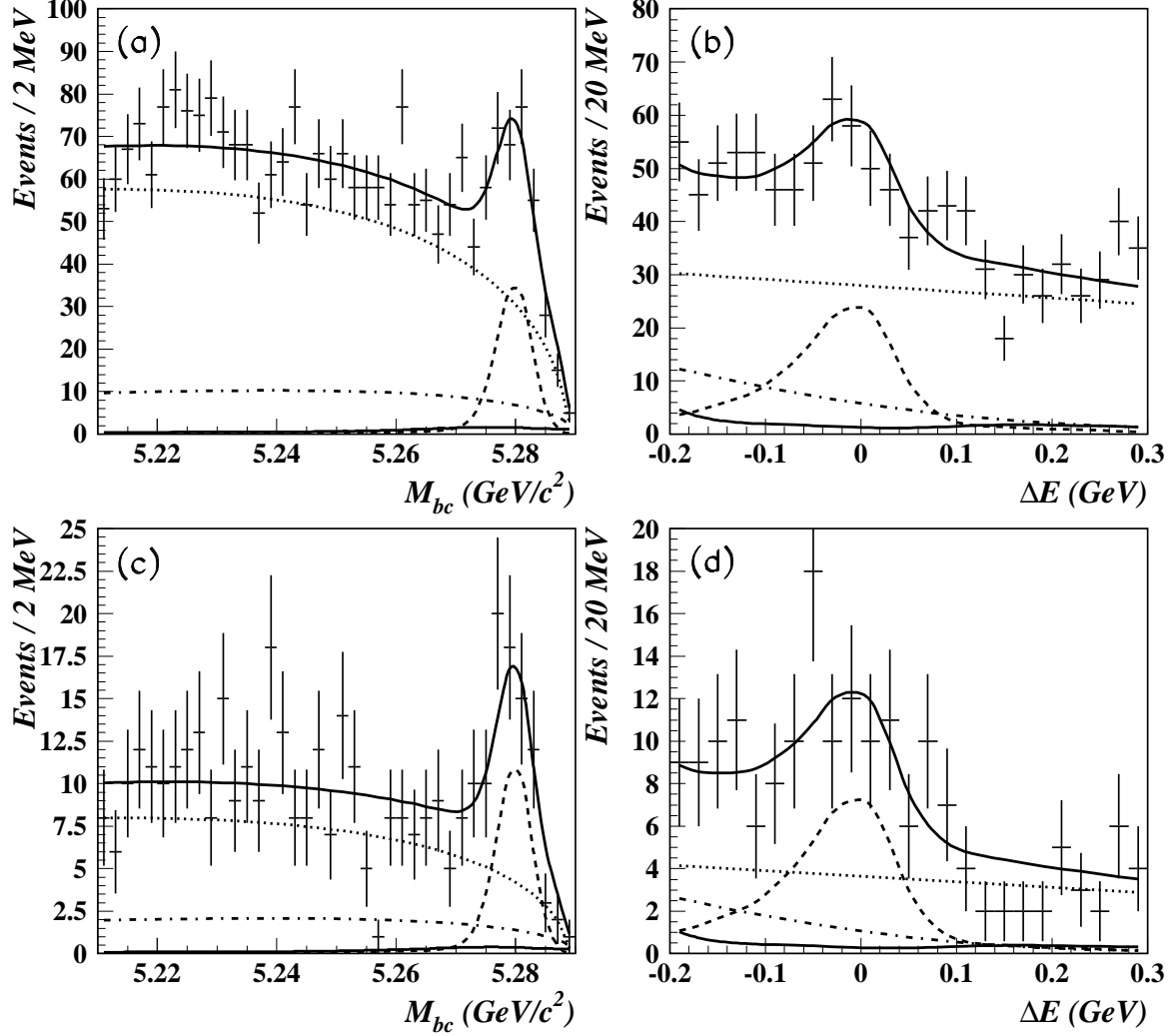


FIG. 1: Left: projection in M_{bc} for events satisfying $-0.10 \text{ GeV} < \Delta E < 0.06 \text{ GeV}$. Right: projection in ΔE for events satisfying $5.273 \text{ GeV}/c^2 < M_{bc} < 5.290 \text{ GeV}/c^2$. The top plots correspond to all r values, and the bottom plots correspond to $0.75 < r < 1.0$. The curves show projections of the ML fit result: the dashed curve represents $\rho^+\rho^- + \rho\pi\pi$ events, the dotted curve represents $q\bar{q}$ background, the dot-dashed curve represents $b \rightarrow c$ background, the small solid curve represents $b \rightarrow u$ background, and the large solid curve shows the overall result.

The different sources and the corresponding changes are: track reconstruction efficiency (1.2% per track); π^0 reconstruction efficiency (4% per π^0); the π^\pm identification efficiency ε_{PID} in Eq. (1) (1.4%); MC statistics used to calculate the acceptance ε in Eq. (1) (1.0%); the dependence of the acceptance upon f_L (+0.0%, -4.1%); the continuum suppression requirement (13%); and the fraction of signal+non-resonant decays used as a constraint in the $m_{\pi^\pm\pi^0}$ fit. This last error itself has several components: the calibration factors used to correct the M_{bc} - ΔE distribution of MC $B^0 \rightarrow \rho^+\rho^-$ events (to better match the data); the M_{bc} - ΔE shapes used for $b \rightarrow c$ background; the fraction of $b \rightarrow u$ background, which is obtained from MC simulation and includes several estimated branching fractions; and the ΔE range used in the fit. These components give an overall variation in $f_{\rho\rho} + f_{\rho\pi\pi}$ of (+2.9%, -8.6%). We subsequently redo the $m_{\pi^\pm\pi^0}$ fit, varying $f_{\rho\rho} + f_{\rho\pi\pi}$ by this amount; the

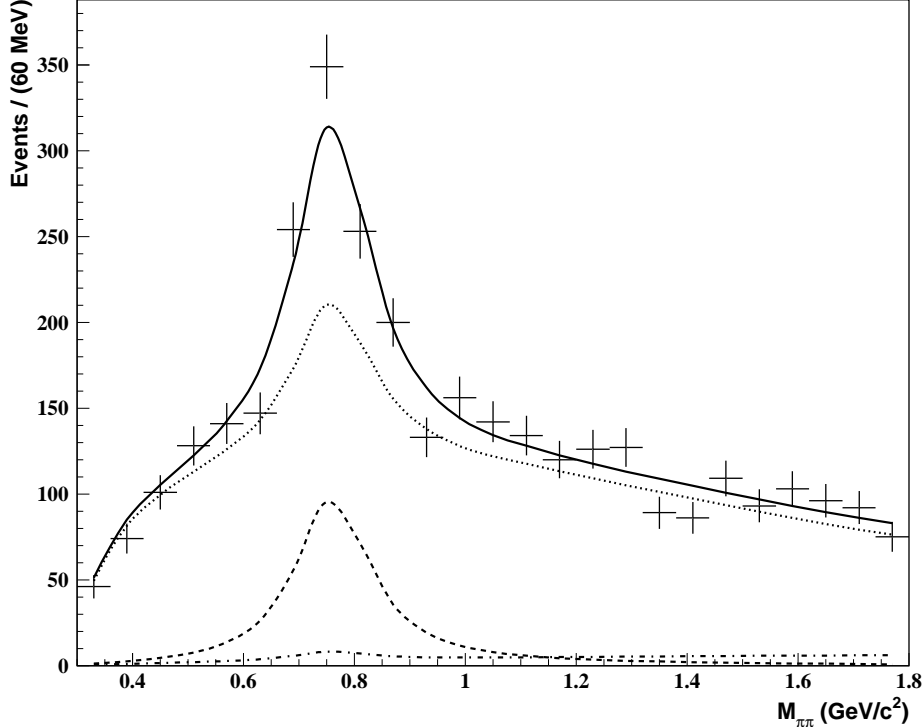


FIG. 2: The $m_{\pi^+\pi^0}$ plus $m_{\pi^-\pi^0}$ distribution (two entries per event) for events satisfying $5.27 \text{ GeV}/c^2 < M_{bc} < 5.29 \text{ GeV}/c^2$ and $-0.12 \text{ GeV} < \Delta E < 0.08 \text{ GeV}$. Superimposed are projections of the ML fit result. The dashed curve represents $\rho^+\rho^-$ signal; the dot-dashed curve represents non-resonant $\rho\pi\pi$ decays; the dotted curve represents $q\bar{q} + (b \rightarrow c) + (b \rightarrow u)$ backgrounds; and the solid curve shows the overall result.

resulting change in $N_{\rho\rho}$ is (+2.0%, -6.4%). Combining this in quadrature with the other systematic errors gives an overall systematic error of (+16%, -17%). Thus the final result for the branching fraction is

$$B(B^0 \rightarrow \rho^+\rho^-) = \left[24.4 \pm 2.2 (\text{stat}) {}^{+3.8}_{-4.1} (\text{syst}) \right] \times 10^{-6}. \quad (2)$$

To determine the polarization of $B^0 \rightarrow \rho^+\rho^-$ decays, we do an unbinned ML fit to the helicity angle distribution $F(\cos\theta_1, \cos\theta_2)$, where θ_1 (θ_2) is the angle between the direction of the π^0 from the ρ^+ (ρ^-) and the negative of the B^0 momentum in the ρ^+ (ρ^-) rest frame. For a longitudinal polarization fraction f_L , this distribution is

$$\frac{9}{4} \left[f_L \cos^2\theta_1 \cos^2\theta_2 + \frac{1}{4}(1 - f_L) \sin^2\theta_1 \sin^2\theta_2 \right]. \quad (3)$$

In the fit, this PDF is multiplied by a two-dimensional acceptance function for $(\cos\theta_1, \cos\theta_2)$ determined from MC simulation. The acceptance is modeled as the product $A(\cos\theta_1) \cdot A(\cos\theta_2)$, where A is a polynomial function.

We fit events satisfying $5.27 \text{ GeV}/c^2 < M_{bc} < 5.29 \text{ GeV}/c^2$, $-0.12 \text{ GeV} < \Delta E < 0.08 \text{ GeV}$, and $0.62 \text{ GeV}/c^2 < m_{\pi^\pm\pi^0} < 0.92 \text{ GeV}/c^2$. The likelihood function includes PDFs for signal, $\rho\pi\pi$ non-resonant decays, and continuum, $b \rightarrow c$, and $b \rightarrow u$ backgrounds. The PDF for non-resonant decays is taken to be constant, and the PDF for $b \rightarrow u$ background is taken from MC

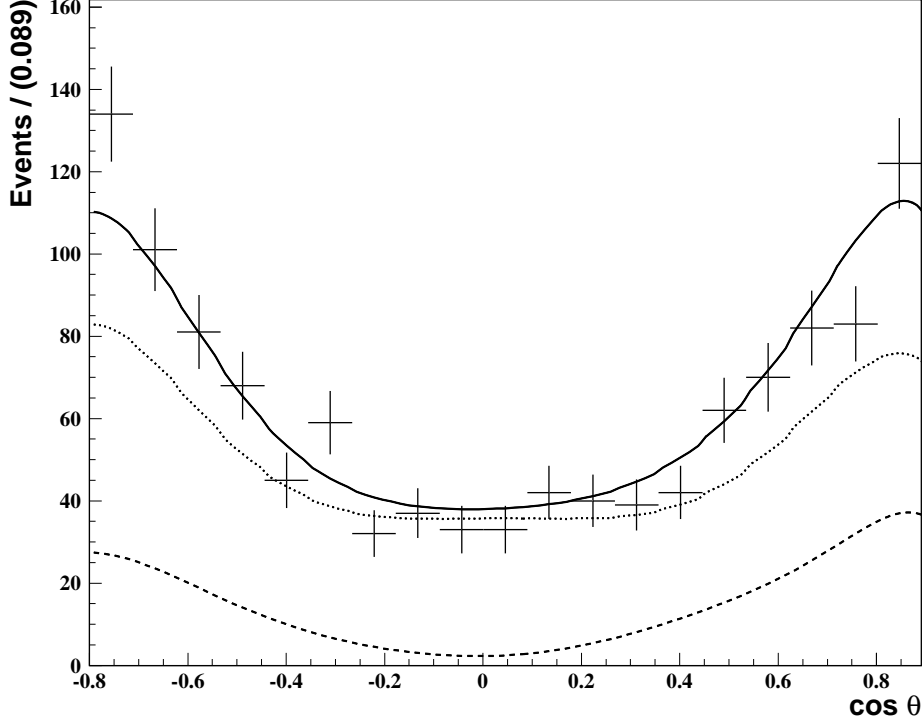


FIG. 3: The $\cos\theta_1$ plus $\cos\theta_2$ distribution (two entries per event) for events satisfying $5.27 \text{ GeV}/c^2 < M_{bc} < 5.29 \text{ GeV}/c^2$, $-0.12 \text{ GeV} < \Delta E < 0.08 \text{ GeV}$, and $0.62 \text{ GeV}/c^2 < m_{\pi^\pm\pi^0} < 0.92 \text{ GeV}/c^2$. Superimposed are projections of the ML fit result. The dashed curve represents $\rho^+\rho^-$ signal; the dotted curve represents non-resonant $\rho\pi\pi$ decays and $q\bar{q} + (b \rightarrow c) + (b \rightarrow u)$ backgrounds, and the solid curve shows the overall result.

simulation. The PDFs for continuum and $b \rightarrow c$ backgrounds are combined and determined from the data sideband $5.21 \text{ GeV}/c^2 < M_{bc} < 5.26 \text{ GeV}/c^2$, $-0.12 \text{ GeV} < \Delta E < 0.12 \text{ GeV}$; we use MC simulation to check that the shapes of these backgrounds and their ratio in the sideband region are very close those in the signal region. The fraction of signal + non-resonant decays is taken from the previous $M_{bc}-\Delta E$ fit; the component $f_{\rho\pi\pi}$ is taken from the previous $m_{\pi^\pm\pi^0}$ fit. The fraction of $b \rightarrow u$ background is small and is taken from MC simulation. Since $f_{(q\bar{q}+b \rightarrow c)} = 1 - f_{\rho\rho} - f_{\rho\pi\pi} - f_{b \rightarrow u}$, there is only one free parameter in the fit (f_L). The result of the fit is $f_L = 0.951^{+0.033}_{-0.039}$, where the error given is statistical. Figure 3 shows the data and projections of the fit result. The χ^2 of the fit projections divided by the number of bins is 0.83 for $\cos\theta_1$ and 1.05 for $\cos\theta_2$.

For this measurement there are eight sources of systematic error; their effect is evaluated by varying the relevant parameter(s) by $\pm 1\sigma$ and noting the resulting change in f_L . The different sources and the corresponding changes are: the signal + non-resonant fraction (+0.013, -0.012); the non-resonant fraction (+0.021, -0.020); the pion identification efficiency, which has a small effect upon the acceptance (+0.000, -0.004); misreconstructed $B^0 \rightarrow \rho^+\rho^-$ decays (+0.005, -0.000); the continuum suppression requirement (± 0.013); possible interference with an $L = 0$ $\pi^\pm\pi^0$ system produced in non-resonant $\rho^\pm\pi^\mp\pi^0$ decays (± 0.005); a very small bias in the fitting procedure measured from a large toy MC sample (+0.000, -0.005); and uncertainty in the continuum + ($b \rightarrow c$) background shape (+0.004, -0.014). This last uncertainty is evaluated by taking the background shape from

alternative M_{bc} and ΔE sidebands. Combining all systematic errors in quadrature gives an overall systematic error of $(+0.029, -0.031)$. Thus the final result for the fraction of longitudinally polarized decays is

$$f_L = 0.951^{+0.033}_{-0.039} (\text{stat})^{+0.029}_{-0.031} (\text{syst}). \quad (4)$$

To fit for the CP asymmetry coefficients \mathcal{A} and \mathcal{S} , we divide the data into $q = +1$ and $q = -1$ tagged decays and do an unbinned ML fit to the respective Δt distributions. At KEKB, the $\Upsilon(4S)$ is produced with a Lorentz boost of $\beta\gamma = 0.425$ nearly along the electron beamline (z); since the B^0 and \bar{B}^0 mesons are approximately at rest in the e^+e^- CM frame, Δt is determined from the displacement in z between the f_{CP} and f_{tag} decay vertices: $\Delta t \approx (z_{CP} - z_{\text{tag}})/\beta\gamma c$.

The likelihood function for event i is

$$\begin{aligned} \mathcal{L}_i = & f_{\rho\rho}^{(i)} \mathcal{P}(\Delta t)_{\rho\rho} + f_{\text{SCF}}^{(i)} \mathcal{P}(\Delta t)_{\text{SCF}} + f_{\rho\pi\pi}^{(i)} \mathcal{P}(\Delta t)_{\rho\pi\pi} + \\ & f_{b\rightarrow c}^{(i)} \mathcal{P}(\Delta t)_{b\rightarrow c} + f_{b\rightarrow u}^{(i)} \mathcal{P}(\Delta t)_{b\rightarrow u} + f_{q\bar{q}}^{(i)} \mathcal{P}(\Delta t)_{q\bar{q}}, \end{aligned} \quad (5)$$

where the event weights $f^{(i)}$ are functions of M_{bc} and ΔE and are normalized to the fractions of events obtained from the previous M_{bc} - ΔE and $m_{\pi^\pm\pi^0}$ fits. The PDFs $\mathcal{P}(\Delta t)$ for $b \rightarrow c$ and $b \rightarrow u$ backgrounds are determined from MC simulation, and the PDF for continuum $q\bar{q}$ background is determined from an M_{bc} sideband. We include an additional PDF for SCF background in which a π^\pm daughter is swapped with a track from the rest of the event; this function is determined from MC simulation and is found to be exponential with an effective lifetime of about 1 ps. The weighting function f_{SCF} is also determined from MC simulation; its normalization is 5.7% of all $\rho^+\rho^-$ candidates.

The PDF $\mathcal{P}_{\rho\rho}(\Delta t)$ is given by

$$\int_{-\infty}^{+\infty} \frac{e^{-|\Delta t'|/\tau_{B^0}}}{4\tau_{B^0}} \left\{ 1 - q \Delta\omega_{\ell(i)} + q(1 - 2\omega_{\ell(i)}) \times \right. \\ \left. [\mathcal{A} \cos(\Delta m \Delta t') + \mathcal{S} \sin(\Delta m \Delta t')] \right\} R(\Delta t^{(i)}, \Delta t') d\Delta t', \quad (6)$$

where $R(\Delta t, \Delta t')$ is a resolution function determined from data, ω_ℓ is the mistag probability for the ℓ th bin of the tagging parameter r , and $\Delta\omega_\ell$ is a possible difference in ω_ℓ between $q = +1$ and $q = -1$ tags. The PDF $\mathcal{P}_{\rho\pi\pi}$ is taken to be exponential with $\tau = \tau_B$ and is smeared by the same resolution function R . We determine \mathcal{A} and \mathcal{S} by maximizing the log-likelihood $\sum_i \log \mathcal{L}_i$, where i runs over the 656 candidate events satisfying $5.27 \text{ GeV}/c^2 < M_{bc} < 5.29 \text{ GeV}/c^2$, $-0.12 \text{ GeV} < \Delta E < 0.08 \text{ GeV}$, and $0.62 \text{ GeV}/c^2 < m_{\pi^\pm\pi^0} < 0.92 \text{ GeV}/c^2$. The results of the fit are $\mathcal{A} = 0.00 \pm 0.30$ and $\mathcal{S} = 0.09 \pm 0.42$, where the errors given are statistical. These values are consistent with the no- CP -violation case $\mathcal{A} = \mathcal{S} = 0$, and the errors are consistent with expectations based on MC studies. Figure 4 shows the data and projections of the fit result for $0.0 < r < 0.5$ and $0.5 < r < 1.0$ subsamples; the χ^2 of the projections divided by the number of bins is 0.98 and 0.97, respectively, which is satisfactory.

For this measurement there are twelve sources of systematic error; their effect is evaluated by varying the relevant parameter(s) by $\pm 1\sigma$ and noting the resulting change in \mathcal{A} and \mathcal{S} . The different sources and the corresponding changes are listed in Table I. The error due to wrong-tag fractions is evaluated by varying ω_ℓ and $\Delta\omega_\ell$ values. The error due to $b \rightarrow c$ and continuum Δt distributions is evaluated by varying the ~ 40 parameters used to describe

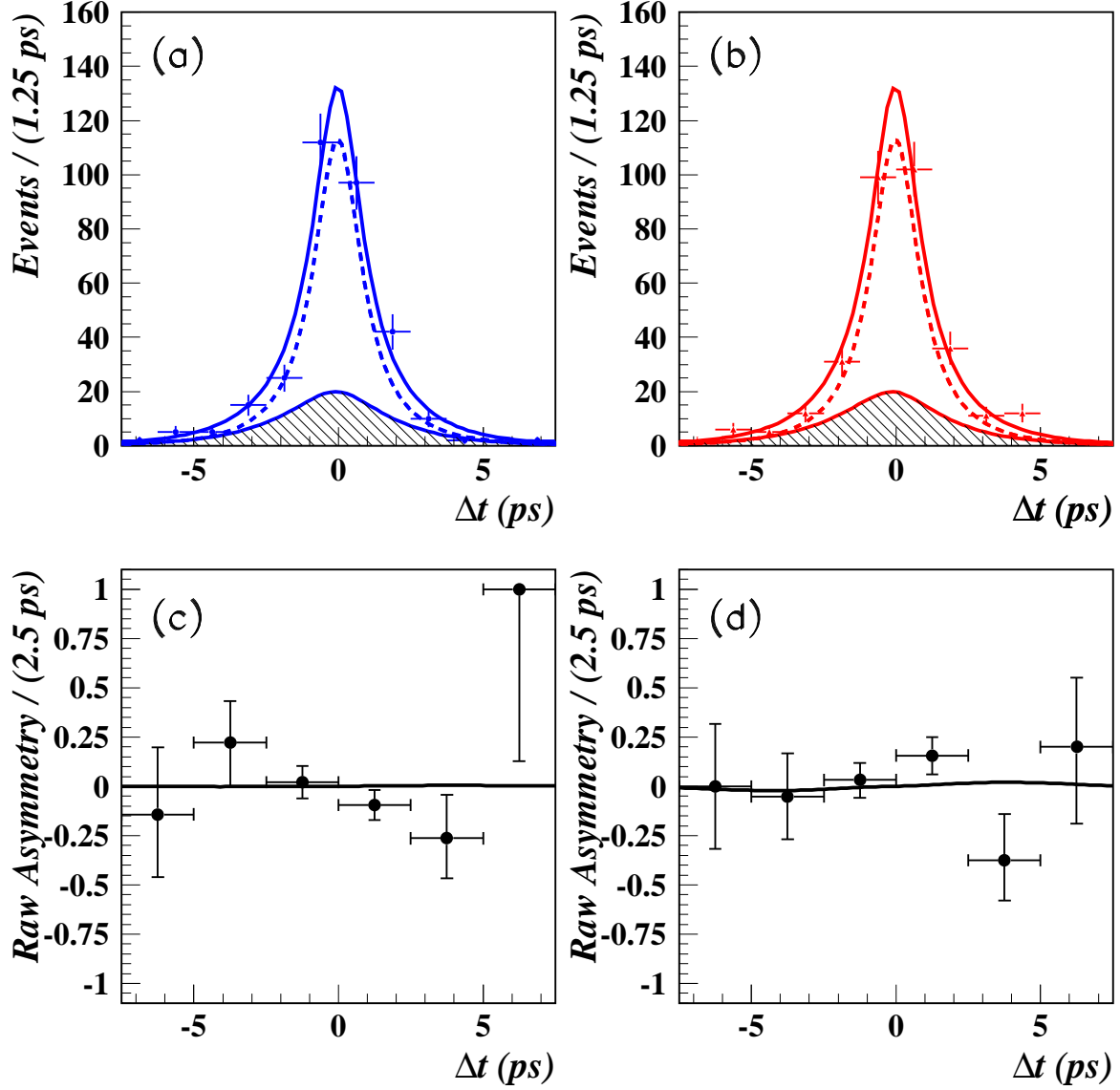


FIG. 4: The Δt distribution for events satisfying $5.27 \text{ GeV}/c^2 < M_{bc} < 5.29 \text{ GeV}/c^2$, $-0.12 \text{ GeV} < \Delta E < 0.08 \text{ GeV}$, and $0.62 \text{ GeV}/c^2 < m_{\pi^{\pm}\pi^0} < 0.92 \text{ GeV}/c^2$. Superimposed are projections of the ML fit result. **(a)** $q=+1$ tags; **(b)** $q=-1$ tags; **(c)** raw CP asymmetry for $0.0 < r < 0.5$; **(d)** raw CP asymmetry for $0.5 < r < 1.0$. For **(a)** and **(b)**, the hatched distribution represents signal events and the dashed curve represents background.

these distributions. The error due to the component fractions is evaluated by varying the fractions obtained from the $M_{bc}-\Delta E$ fit. The error due to self-cross-feed (SCF) events is evaluated by varying both the SCF fraction (by 50%) and the effective lifetime used for SCF events (by 2σ). The effect of a CP asymmetry in $b \rightarrow c$ and $q\bar{q}$ backgrounds is evaluated by adding such asymmetries to the $b \rightarrow c$ and $q\bar{q}$ Δt distributions; the sizes of these asymmetries are taken to be those obtained from fitting an M_{bc} sideband in the data (these values are small and consistent with zero). The error due to a possible fitting bias is evaluated using a full MC simulation, and the error due to tag-side interference [9] is evaluated using a toy MC simulation. The error due to the transversity amplitudes A_{\perp} and A_{\parallel} (which may have

different values of \mathcal{A} and \mathcal{S}) is evaluated in two steps: first setting f_L equal to its central value and varying the values of $(\mathcal{A}, \mathcal{S})$ for A_\perp and A_\parallel over the range -1 to $+1$; second, using common values of $(\mathcal{A}, \mathcal{S})$ for all transversity amplitudes (except for an extra minus sign for A_\perp) and varying f_L . Combining all systematic errors in quadrature gives overall systematic errors of $(+0.10, -0.09)$ for \mathcal{A} and ± 0.08 for \mathcal{S} . Thus the final result is

$$\mathcal{A} = 0.00 \pm 0.30 \text{ (stat)} \begin{matrix} +0.10 \\ -0.09 \end{matrix} \text{ (syst)} \quad (7)$$

$$\mathcal{S} = 0.09 \pm 0.42 \text{ (stat)} \pm 0.08 \text{ (syst)}. \quad (8)$$

TABLE I: Systematic errors for the CP asymmetry coefficients \mathcal{A} and \mathcal{S} .

Type	$\delta\mathcal{A} (\times 10^{-2})$		$\delta\mathcal{S} (\times 10^{-2})$	
	$+\sigma$	$-\sigma$	$+\sigma$	$-\sigma$
Wrong tag fractions	0.5	0.6	0.8	0.8
Parameters $\Delta m, \tau_{B^0}$	0.1	0.1	0.9	0.9
Resolution function	1.3	1.3	1.3	1.3
Background Δt distributions	1.6	1.5	2.3	2.5
Component fractions	2.1	2.6	5.0	4.5
$\rho\pi\pi$ non-resonant fraction	0.0	0.0	0.6	0.6
Self-cross-feed (SCF) fraction	0.0	0.0	0.2	0.2
Background asymmetry	0.0	2.0	0.0	4.3
Possible fitting bias	0.0	0.2	0.6	0.0
Vertexing	4.1	2.8	0.4	0.4
Tag-side interference	7.2	5.5	0.3	0.0
f_\perp, f_\parallel (transversely-polarized components)	5.2	4.5	6.0	4.7
Total	+10.2	-8.6	+8.4	-8.4

We use these values along with the measured branching fraction for $B^0 \rightarrow \rho^+\rho^-$ and previously-measured branching fractions for $B^+ \rightarrow \rho^+\rho^0$ [10] and $B^0 \rightarrow \rho^0\rho^0$ [2] to constrain the angle ϕ_2 . We use the isospin relations of Ref. [11] (originally applied to the $B \rightarrow \pi\pi$ system), neglecting a possible $I=1$ contribution to the $B^0 \rightarrow \rho^+\rho^-$ amplitude [12]. We first fit the measurements to obtain a minimum χ^2 ; this is denoted χ_{\min}^2 . We then scan values of ϕ_2 from 0° – 180° and for each value calculate the difference $\Delta\chi^2 \equiv \chi^2(\phi_2) - \chi_{\min}^2$. We insert $\Delta\chi^2$ into the cumulative distribution function for the χ^2 distribution for one degree of freedom to obtain the confidence level (CL) for the ϕ_2 value. The curve 1 –CL for all ϕ_2 values is plotted in Fig. 5. From this curve we obtain a central value and 1σ error $\phi_2 = (87 \pm 17)^\circ$; the 90% CL interval around the central value is $59^\circ < \phi_2 < 115^\circ$.

In summary, we have measured the branching fraction, longitudinal polarization fraction f_L , and CP asymmetry coefficients \mathcal{A} and \mathcal{S} for $B^0 \rightarrow \rho^+\rho^-$ decays. Our results are $B = [24.4 \pm 2.2 \begin{matrix} +3.8 \\ -4.1 \end{matrix}] \times 10^{-6}$, $f_L = 0.951 \begin{matrix} +0.033 & +0.029 \\ -0.039 & -0.031 \end{matrix}$, $\mathcal{A} = 0.00 \pm 0.30 \begin{matrix} +0.10 \\ -0.09 \end{matrix}$, and $\mathcal{S} = 0.09 \pm 0.42 \pm 0.08$, where the first error listed is statistical and the second error listed is systematic. These

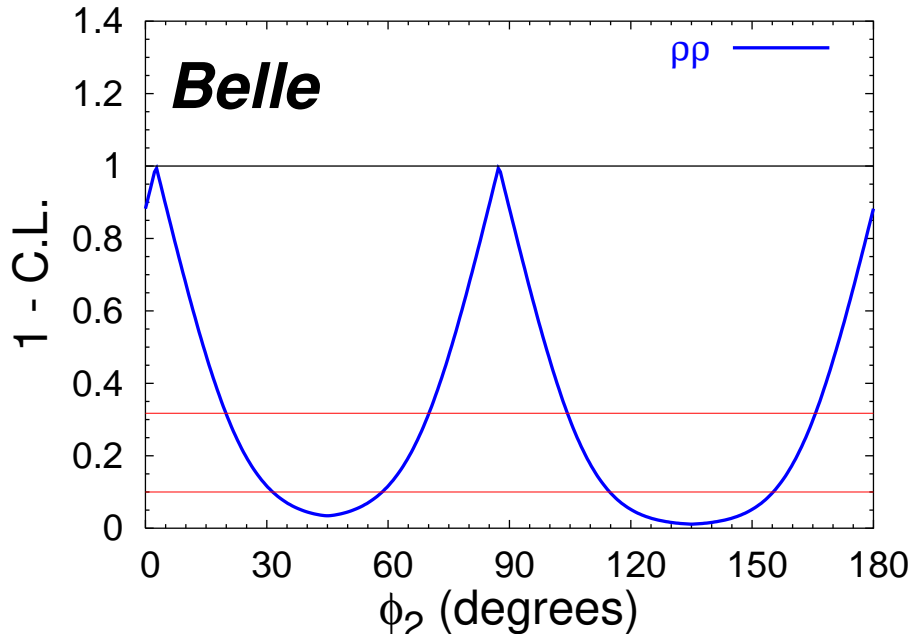


FIG. 5: Results of fitting the branching fractions $B(B^0 \rightarrow \rho^+\rho^-)$, $B(B^+ \rightarrow \rho^+\rho^0)$, $B(B^0 \rightarrow \rho^0\rho^0)$, and the $\rho^+\rho^-$ asymmetry parameters \mathcal{A} and \mathcal{S} for the angle ϕ_2 , using the isospin relations of Ref. [11]. The vertical axis is one minus the confidence level (see text). The horizontal line at $1-\text{CL}=0.317$ corresponds to a 68.3% CL interval for ϕ_2 , and the horizontal line at $1-\text{CL}=0.10$ corresponds to a 90% CL interval.

results are consistent with previously-published measurements [13]. The result for f_L is consistent with the theoretical expectation based on QCD factorization [14], and the results for \mathcal{A} and \mathcal{S} are consistent with the case of no CP violation. From an isospin analysis we obtain the constraint $59^\circ < \phi_2 < 115^\circ$ at 90% CL.

We thank the KEKB group for the excellent operation of the accelerator, the KEK cryogenics group for the efficient operation of the solenoid, and the KEK computer group and the National Institute of Informatics for valuable computing and Super-SINET network support. We acknowledge support from the Ministry of Education, Culture, Sports, Science, and Technology of Japan and the Japan Society for the Promotion of Science; the Australian Research Council and the Australian Department of Education, Science and Training; the National Science Foundation of China under contract No. 10175071; the Department of Science and Technology of India; the BK21 program of the Ministry of Education of Korea and the CHEP SRC program of the Korea Science and Engineering Foundation; the Polish State Committee for Scientific Research under contract No. 2P03B 01324; the Ministry of Science and Technology of the Russian Federation; the Ministry of Higher Education, Science and Technology of the Republic of Slovenia; the Swiss National Science Foundation; the National Science Council and the Ministry of Education of Taiwan; and the U.S. Department of Energy.

-
- [1] The naming convention α ($= \phi_2$), β ($= \phi_1$), and γ ($= \phi_3$) is also used in the literature.
- [2] B. Aubert *et al.* (BaBar Collaboration), Phys. Rev. Lett. **94**, 131801 (2005).
- [3] S. Kurokawa and E. Kikutani, Nucl. Instr. and Meth. A **499**, 1 (2003), and other papers included in this volume.
- [4] A. Abashian *et al.* (Belle Collaboration), Nucl. Instr. and Meth. A **479**, 117 (2002).
- [5] Y. Ushiroda (Belle SVD2 Group), Nucl. Instr. and Meth. A **511**, 6 (2003).
- [6] H. Kakuno *et al.*, Nucl. Instr. and Meth. A **533**, 516 (2004).
- [7] S. H. Lee *et al.* (Belle Collaboration), Phys. Rev. Lett. **91**, 261801 (2003).
- [8] H. Albrecht *et al.* (ARGUS Collaboration), Phys. Lett. B **241**, 278 (1990).
- [9] O. Long *et al.*, Phys. Rev. D **68**, 034010 (2003).
- [10] S. Eidelman *et al.* (PDG), Phys. Lett. B **592**, 1 (2004).
- [11] M. Gronau and D. London, Phys. Rev. Lett. **65**, 3381 (1990).
- [12] A. Falk *et al.*, Phys. Rev. D **69**, 011502(R) (2004).
- [13] B. Aubert *et al.* (BaBar Collaboration), Phys. Rev. Lett. **93**, 231801 (2004).
- [14] A. Kagan, Phys. Lett. B **601**, 151 (2004).